Nigerian Research Journal of Engineering and Environmental Sciences 5(2) 2020 pp. 726-736

Nigerian Research Journal of Engineering and Environmental Sciences
Journal homepage: www.rjees.com

Original Research Article

Hybrid Concatenation of Emphysema Features for Improving Classification in Computed Tomography Images

***[1]Ibrahim, M.A. and [2]Ojo, O.A.**

[1]Department of ICT, Faculty of Basic and Applied Sciences, Osun State University, Osogbo, Nigeria.
[2]Department of Physics, Faculty of Basic and Applied Sciences, Osun State University, Osogbo, Nigeria.
*kunle_ibrahim2001@yahoo.com

ARTICLE INFORMATION

Article history:
Received 29 Aug, 2020
Revised 02 Oct, 2020
Accepted 09 Oct, 2020
Available online 30 Dec, 2020

Keywords:
Emphysema classification
Multifractal analysis
Multifractal spectrum
Histogram comparison
Statistical self-similarity

ABSTRACT

Previous studies have recently demonstrated the effectiveness of multifractal based methods for the classification of histo-pathological cases by calculating the local singularity coefficients of an image using different intensity measures. In this paper, we propose to improve on the existing results on multifractal techniques by investigating the features from the combination of alpha-histograms and multifractal descriptors in the classification of Emphysema in computed tomography (CT) images. The performances of the classifiers were measured by using classification accuracy (error matrix) and area under curve (AUC). The experimental results compared favourably with the local binary patterns (LBP) approach, a state-of-the-art measure for pulmonary Emphysema. The results also showed that the proposed cascaded approach significantly improved the overall classification accuracy.

1. INTRODUCTION

Emphysema is one of the main components of chronic obstructive pulmonary diseases (COPD) and it is characterized by loss of lung tissue and may eventually lead to gradual destruction of lung (Sorensen et al., 2010). Detection and classification of Emphysema are therefore very important as this may lead to improved computer-aided diagnosis (CAD) (Chabat and Yang,2003). Diagnosing Emphysema usually requires pulmonary function tests (PFTs), combined with a history of symptoms. The main tool through which the tests are performed is the spirometer. However, PFTs are not capable of detecting COPD at early stages. Another popular tool for diagnosing Emphysema is high resolution computed tomography (HRCT) imaging. The presence, distribution and extent of Emphysema patterns in images can also be demonstrated using a suitable computed tomography (CT) imaging (Chabat and Yang, 2003).

Emphysema patterns in CT are usually characterized by abnormally low attenuation, which are surrounded by normal lung parenchyma (Sørensen and de Bruijne, 2009). There are three different classes of

Emphysema: centrilobular Emphysema (CLE), paraseptal Emphysema (PSE) and panlobular Emphysema (PLE). The state-of-the-art-method developed by Sorensen using the local binary pattern (LBP) has achieved excellent results in the classification of Emphysema subtypes (Sorensen et al., 2009). The intensity distribution of lung tissue images is highly irregular and does not often permit a direct definition of shape parameters using geometrical descriptors. Biomedical images are associated with statistical self-similarity property, a repetition of form over a variety of scales. Several methods of multifractal analysis of medical images have been suggested and evaluated in different ways (Stojic et al., 2006; Nilsson, 2007; Hemsley and Mukundan, 2009; Tay, 2011; Gavroviska, 2013; Ibrahim and Mukundan, 2014). Hemsley and Mukundan, (2009) developed a two-pass algorithm for the computation of multifractal spectrum and used the calculated spectra for the classification in a tissue image database. In Tay et al. (2011), the Holder exponent for the power law approximation of intensity measures in pixel neighbourhood was used for resolving local density variations in the CT lung images.

The multifractal analysis could find applications in Emphysema classification in CT images of the lung, but not much research has so far been done in this area. Recently, a classification algorithm using multifractal descriptors was proposed (Ibrahim and Mukundan, 2014; Ibrahim et al., 2017a; Ibrahim et al., 2017b). This paper provides an improved method using a combination of two different descriptors (multifractal spectra and alpha-histograms) for obtaining higher accuracy in the results. The first approach combines the features obtained from multifractal descriptors and alpha-histograms in the form of hybrid for the classification process. The second idea uses the area under the receiver operating characteristic (ROC) curves to identify the best features that could yield maximum classification accuracy and high computational efficiency.

2. METHODOLOGY

2.1. Computation of Multifractal Methods

The online CT Emphysema database (Sorensen et al., 2010) used for this research consists of 168 non-overlapping annotated regions of interests (ROIs) of size 61×61 pixel patches from three different classes: NT (59 never-smokers), CLE (50 healthy smokers), and PSE (59 smokers with COPD) (Sorensen et al., 2010). The multifractal based approach for classifying Emphysema patterns in CT images is shown in Figure 1. The first stage involved several algorithmic steps, where the α-values for each pixel using a pre-selected intensity measure were defined across pixel neighborhoods. The details of this computation can be found in section 2.2. Generally speaking, the α-values describe the variation in the local density of the image with respect to the chosen measure. These α-values were therefore gathered together to generate the α-image (Figure 1). The range of α-values was subdivided into a number of small intervals, effectively decomposing the α-image into several disjoint image slices. Each α-image slice represents the collection of pixels in the input image having similar intensity variation (obeying similar power-law relationship in the intensity measure) across the pixel neighborhoods. The traditional box-counting method was used for the calculation of the fractal dimension $f(\alpha)$ of the α-images, providing the multifractal spectrum (Figure 1). Those pixels with similar α-values were combined to obtain α-histogram. Both the α-histogram and the multifractal spectrum contain highly discriminating texture features. Such features were collected to form a descriptor and used as image classifier for detecting emphysema diseases in the CT images.

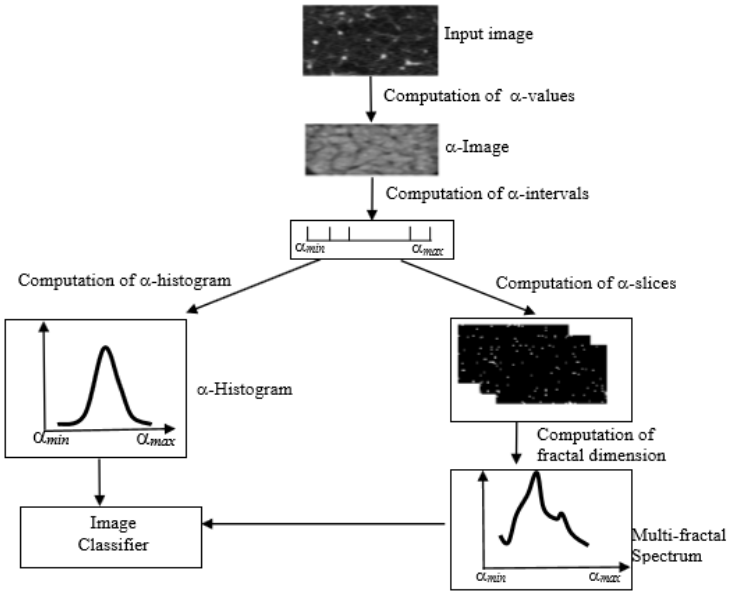

Figure 1: System overview of multifractal based classification of CT

2.2. Holder Exponent and Multifractal Measures

The multifractal analysis describes the fractal properties of an image using an intensity-based measure within the neighborhoods of each pixel. The local singularity coefficient, also known as the Holder exponent (Vehel, 1964; Falconer, 2003; Nilsson, 2007; Mukundan and Hemsley, 2010) reveals the local behaviour of a measure function denoted as $\mu_p(w)$ where w stands for the window size centred at the pixel p (see Figure 2). The variation of the intensity measure with respect to w can be characterized as follows:

$$\mu_p(w) = Cw^{\alpha_p} \quad (1)$$

$$w = 2k + 1,\ k = 0,\ 1,\ 2,\ \cdots,\ m \quad (2)$$

where C is an arbitrary constant, and m is the total number of boxes used in the computation of α_p. The value of α_p can be estimated from the slope of the linear regression line in a log-log plot where $\log(\mu_p(w))$ is plotted against $\log(w)$. Some commonly used multifractal intensity measures used for the computation of the Holder exponent are the summation measure, the iso-surface measure, the maximum intensity measure and the inverse minimum measure. The final multifractal spectrum computed from an image obviously depends on the choice of the intensity-based measure that represents local variations of intensity values.

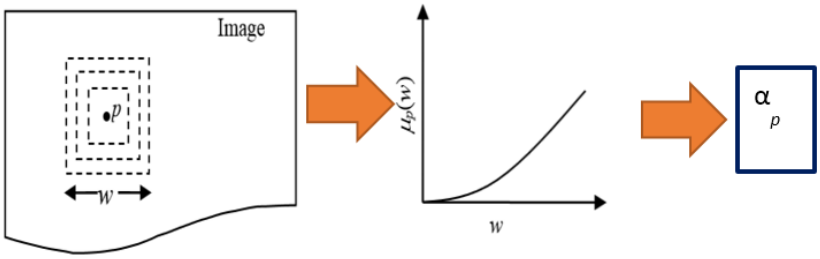

Figure 2: The Holder exponent is computed across multiple windows

A brief description of the intensity measure is given below. The sum measure $\mu_p^{[sum]}(w)$ is defined as the sum of the intensity measure within a local neighbourhood w (Equation 3). The measure could be further normalized using the total mass intensity. The normalized measure prevents values from becoming exceedingly large, which may lead to numerical instability (Choi and Lee, 2003; Hemsley, 2009; Ibrahim and Mukundan, 2014; Ibrahim et al., 2017a; Ibrahim et al., 2017b).

$$\mu_p^{[sum](w)} = \sum_{q \in w} I_q \tag{3}$$

where I_q denotes the intensity value at a pixel q within the window w. The iso measure $\mu_p^{[iso]}(w)$ counts the number of pixels that have the same intensity value with the centred pixel p in a neighborhood. If the centred pixel is the only pixel with unique intensity in the region, then measure has a value 1.

$$\mu_p^{[iso]}(w) = \{qI_q \cong I_q; q \in w\} \tag{4}$$

where # is the number of pixels. To account for minor variations in intensity values and noise, a threshold is often used in the comparison in Equation (4). The inverse-minimum measure is $\mu_p^{[min]}(w)$ defined as follows:

$$\mu_p^{[min]}(w) = 1 - min_{q \in w} I_q \tag{5}$$

In Equation (5), the intensity values are assumed to be normalized in the range [0 1], so that the value resulting from the subtraction is always positive. The subtraction from 1 is used to meet the requirement that the measure does not decrease in value with increasing window size. The maximum measure is the measure with the greatest intensity found in the window w centred at the pixel (p) (Equation 6).

$$\mu_p^{[min]}(w) = max_{q \in w} I_q \tag{6}$$

2.3. α-Images and the Multifractal Spectrum

The α_p values at pixels p obtained from the previous step define a range $[\alpha_{\min}, \alpha_{\max}]$ of the real line, which is further divided into n discrete steps $\alpha_1, \alpha_2, \alpha_3, , \alpha_n$. Each intermediate value α_k is defined as follows:

$$\alpha_k = \alpha_{min} + (k-1)\alpha_k,\ k = 1, 2, \cdots, n \tag{7}$$

$$\Delta\alpha_k = (\alpha_{max} - \alpha_{min})/n \tag{8}$$

In this research work, the value n = 100 was used for the experimental analysis in computation of the spectrum. The following images and histogram values are readily obtained:

$\propto -image$:

$$I_p^{\propto} = \left(\frac{\propto_p - \propto_{min}}{\propto_{max} - \propto_{min}}\right)255 \tag{9}$$

$\propto -Histogram$:

$$h_k = \#\{p | \alpha_p \in [a_k, a_{k+1}]\},\ k = 1, 2, \cdots, n-1 \tag{10}$$

α-slices:

$$A_k = \{ p | \propto_p \in [a_k, a_{k+1}] \}, \; k = 1, 2, \cdots, n-1 \tag{11}$$

An α-slice A_k is a binary image; the only foreground pixels (with maximum intensity value) are those pixels that satisfy the condition in Equation (11). It therefore represents the collection of pixels in the original image where the values of the chosen intensity measure show the same power law variation.

2.4. Multifractal Spectrum

An important texture feature that could be used in classification is the statistical self-similarity property exhibited by the sub-images represented by the α-slices. Each α-slice can be characterized by its fractal dimension. An α-slice A_k *has been subdivided* into a regular grid of boxes with integral box sizes ε. The boxes containing at least one foreground pixel as given in Equation (11) are counted, giving the number $N_k(\varepsilon)$. The box sizes are recursively scaled by half, as per the well-known box-counting algorithm (Falconer, 2003), and the fractal dimension of the α-slice estimated as the slope of the linear regression line on the log-log plot with $\log(\varepsilon)$ along the x-axis, and $\log(N_k(\varepsilon))$ along the y-axis. We denote this fractal dimension by $f(\alpha_k)$. The variation of $f(\alpha_k)$ with α_k, $k = 1, 2, \cdots, n-1$ gives the multifractal spectrum.

3. RESULTS AND DISCUSSION

3.1. Application of Multifractal Descriptors

The results generated in Figure 3 were obtained using all the equations outlined in previous section. For instance, from Equations 1 and 2, the α-values that represent the slope of the graph presented in Figure 2 were calculated. Equations 3, 4, 5 and 6 as explained in section 2.2 were used for the computation of the four intensity measures in multifractal analysis. The multifractal graphs representing these four intensity measures (Inverse-Minimum, Maximum, Summation and Iso) were calculated for each emphysema class (Figure 3). The implementation of Equations 3, 4, 5 and 6 produced the results in Figure 3 to describe the multifractal behaviour of emphysema patterns in the CT images. In order to calculate the fractal dimensions of the CT images at various locations or regions, the α-values were subdivided using Equations 7 and 8 and gathered together with Equations 9 and 10 to produce α-image and α-histogram for improving detection and classification accuracy of emphysema diseases across the CT images. Figure 1 explains the algorithmic steps or procedures on how the multifractal spectrum and the α-histogram were computed. The α-image calculated by Equation (9), α-histogram computed by Equation (10), α-slices calculated by Equation (11) and a sample of multifractal spectrum computed with Equations (1,2,3,4,5,6,7,8,10 and 11) are also presented in Figure 1.

In this section, the experimental results were obtained using images from Emphysema database (Sorensen et al., 2010), based on the implementation of the methods discussed in the previous sections. The feature vectors extracted from the calculated multifractal spectra and the alpha-histograms were used for classification and retrieving purposes. The results of the descriptors derived using four multifractal intensity measures for the classification of three classes of Emphysema images (Section 2.2) are given in Figure 3. The histogram descriptors used for the classification experiments were constructed by dividing the range of α-values generated from the Holder exponent into 100 intervals. The alpha-histogram was calculated for each alpha bin as the number of pixel counts with the α-values within the α-range $[\alpha_i \; \alpha_{i+1}]$.

The average of the alpha-histogram for four randomly selected images was calculated and the feature vectors obtained from the descriptors were trained with the classifier algorithm. The alpha-histograms for each Emphysema class using the summation measure for the computation of Holder exponent are given in Figure 4.

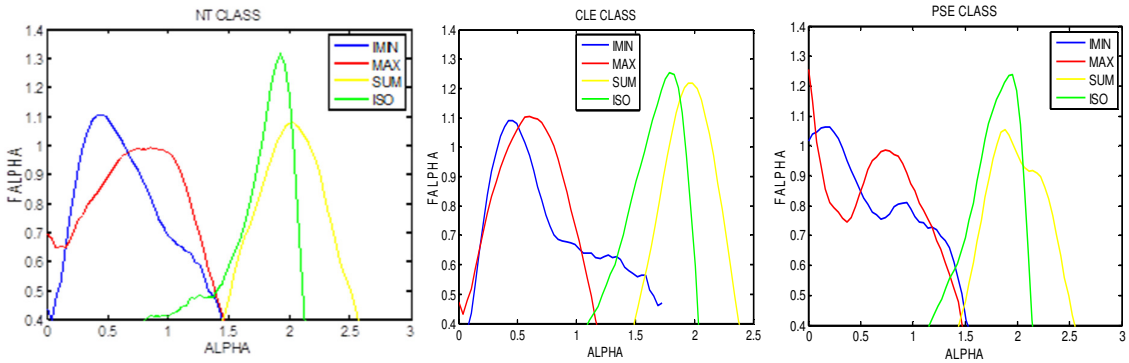

Figure 3: Multifractal descriptors for three classes of Emphysema images using each intensity measure

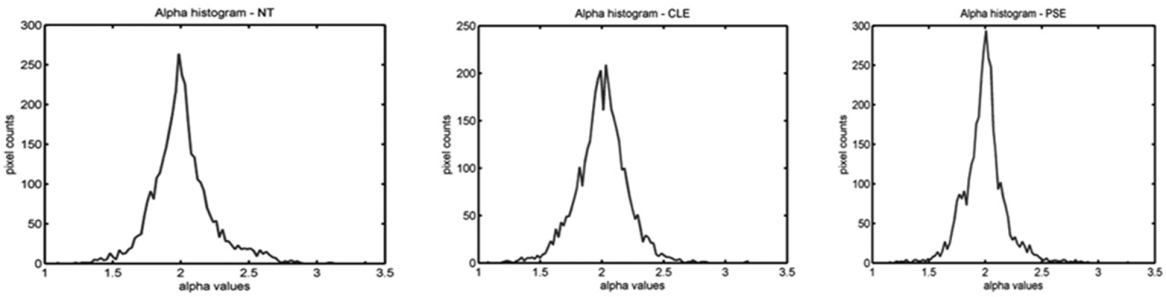

Figure 4: Alpha-histograms of each class of Emphysema image using the summation measure

The first stage of the classification uses the summation intensity measures for the Emphysema classification with different distance metrics (Choi and Lee,2003). The summary of the classification results is shown in Table 1.

Table 1: Classification results using the summation measures

Predicted			
	NT	CLE	PSE
Actual NT	100	0	0
CLE	50	50	0
PSE	17	25	55

It can be observed from the results in Table 1 that there is a clear separation between the normal Emphysema class and other pathological cases, but some CLE classes are misclassified as the normal (NT) classes while some PSE classes also give some classification errors. In the second stage of the classification, the normal Emphysema class is removed such that the alpha-histogram descriptor is used for further classification of the two pathological classes (CLE and PSE). The Naïve Bayes classifier was introduced to this process and the holdout partition method was applied to divide the observations into training sets and test sets (Wang, 2003; Zhang and Su, 2008; Zhang, 2009). There is a scalar specifying the proportion of the number of observations to be randomly selected for validation. In order to achieve promising results since the accuracy of the classifiers majorly depends on the training data; we consider 70 percent of the feature vectors for the training and 30 percent for testing. The performance of the classifiers is evaluated in the form of confusion matrix. A confusion matrix can be represented as a matrix M∈ Rk×k, a square matrix whose diagonal elements represent the actual classification accuracy where k is the number of classes in the dataset. The classification error of the classifiers can be calculated as follows:

$$\text{Error} = 1 - \frac{\text{trace(ConfusionMatrix)}}{\text{Sum(ConfusionMatrix)}} \quad (12)$$

Where trace (.) is the sum of all the elements in the diagonal, and sum (.) is the sum of all the entries in the confusion matrix. The classification results obtained using the Naïve Bayes classifier over the alpha-histograms datasets are presented in Table 2.

Table 2: Classification results for the two pathological classes

		Predicted Alpha-Histogram descriptor	
		CLE	PSE
Actual	CLE	92	8
	PSE	8	92

The entries in the diagonal cells of the Tables presented are the percentage of the instances that are correctly classified, where the actual class matches the predicted classes, the entries off the diagonal are the percentage of the cases that are wrongly classified. The results presented in Table 2 show good performance but with few errors. The next stage of the experiment would be to cascade this current result with the previous results obtained from the multifractal descriptors. The outlines of the experimental procedures are given in Figure 5.

It is noted from the results in Table 2 that the combination of information from the local singularity of the image (the alpha-histograms), combined with the information extracted from the multifractal descriptors, that is, the global features would form a powerful discriminating feature for the Emphysema classification. That is the reason for combining the results from the first stage of the classification to the second stage of the classification, and the final classification outputs are presented in Table 3.

The best two approaches investigated in (Sorensen et al.,2010) are the LBP with an estimated classification accuracy of 95.2%, and the Gaussian filter bank (GFB) histogram with an estimated accuracy of 94%. The overall classification accuracy of 94.7% (Table 3) achieved by the proposed approach compared well with the best two approaches. The LBP result is slightly better, but gives few errors in separating the normal class from other pathological cases, 7% of the normal class are misclassified as PSE class. The results obtained in this work clearly separated the normal class from the pathological cases (CLE and PSE), and outperformed the results achieved by the GFB approach. However, the results of the cascaded method indicate that the CLE and PSE classes have a higher number of misclassification errors than the GFB_LBP.

The results in Table 3 were achieved by direct combination of the results from the multifractal data sets in Table 1 and the classification results generated by the alpha-histogram descriptors in Table 2. The two cells in Table 3 are marked with the asterisk symbol, indicating there are no results between the pathological cases (CLE and PSE) and the normal Emphysema class (NT), since it has been eliminated from the data sets. The results achieved by this proposal show excellent performance with the overall classification accuracy of 94.7% (see Table 3). The final results are then compared with the best two approaches used in the recently published paper (Sorensen et al., 2010) as presented in Table 4.

The performances of the descriptors obtained from the alpha-histograms and the multifractal are also evaluated using the weighted area under the ROC curves. The area under the ROC curve is calculated for all possible combinations of the Emphysema class labels over the data sets derived from the hybrid combination of the alpha-histogram and the multifractal descriptors by using the Wilcoxon rank sum test. The average of the AUC for the possible class pair is calculated for each column and the column with the maximum AUC's value is chosen as the best feature (see Table 5).

Figure 6 presented the ROC curves for the selected features of the data sets and the corresponding class comparison of the AUC are given in Table 5.

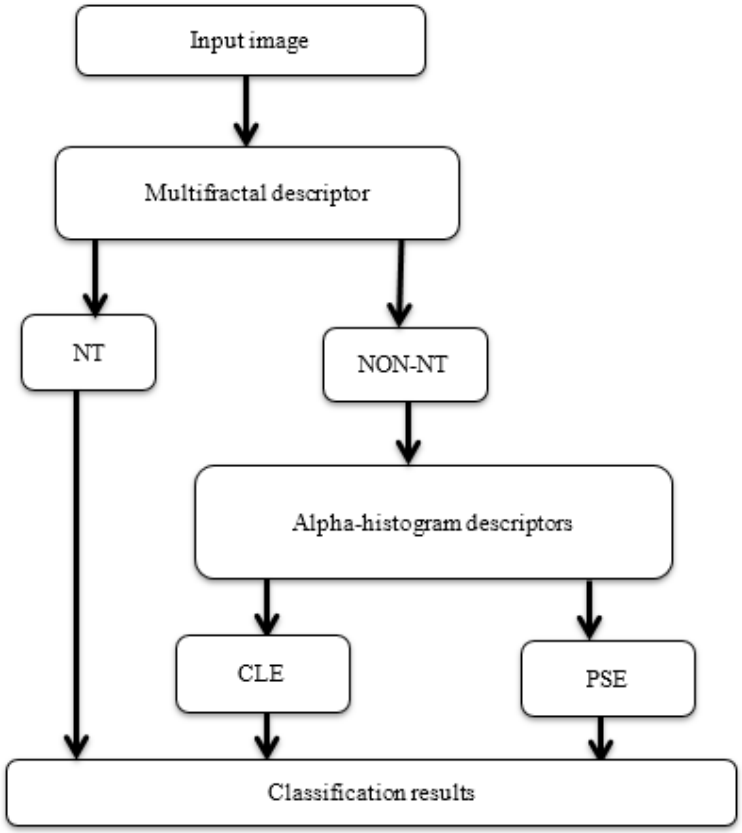

Figure 5: Outline of the experimental procedures for classification

Table 3: Classification results after combining the results from the two stages

		Predicted Final classification outputs		
		NT	CLE	PSE
Actual	NT	100	0	0
	CLE	*	92	8
	PSE	*	8	92

Table 4: Comparison of classification results using cascaded approach and LBP

		Predicted								
	GFB				LBP			Our results		
		NT	CLE	PSE	NT	CLE	PSE	NT	CLE	PSE
Actual	NT	93	0	7	93	0	7	100	0	0
	CLE	4	96	0	2	98	0	*	92	8
	PSE	7	0	93	3	2	95	*	8	92

Table 5: Pairwise AUCs for Emphysema classes

Class comparison	NT VS CLE	NT VS PSE	CLE VS PSE	MEAN AUC
Best feature	0.9204	0.7915	0.7633	0.8251

The Table 6 was generated from the pairwise class comparison results presented in Table 5 by adding the AUCs of the NT versus CLE and the NT versus PSE classes to produce NT versus other cases as indicated in Table 6. The closer the AUC's values to 1, the better the performance of the data sets. It can be noted from the outcomes in Table 6 that the performances of the NT class versus other classes (CLE & PSE) are better than the CLE class versus PSE class using the selected best features.

Table 6: AUCs for normal class *vs.* other cases and CLE *vs.* PSE

Class comparison	NT vs. Others (Ours)	NT vs. PSE	NT vs. Others
AUCs	0.8559	0.7633	0.713

This is also demonstrated in Figure 6, the ROC curves of the NT class versus the CLE class are more separated than the ROC curve for the CLE class versus PSE class. The mean AUC of 0.8251, obtained by averaging all of the pairwise values in Table 5 was used for the selection of the best features. The result in Table 6 is then compared with some recent papers (Sorensen and Bruijine, 2008; Sorensen et al., 2011). In Sorensen et al. (2011), the region of interest classification for discriminating the Emphysema with and without COPD is calculated using the *k* nearest neighbour approach and the AUC of 0.713 is achieved. In comparison with our results, the AUC value of 0.8559 obtained is significantly better than the 0.713 achieved by Sorensen et al. (2011).

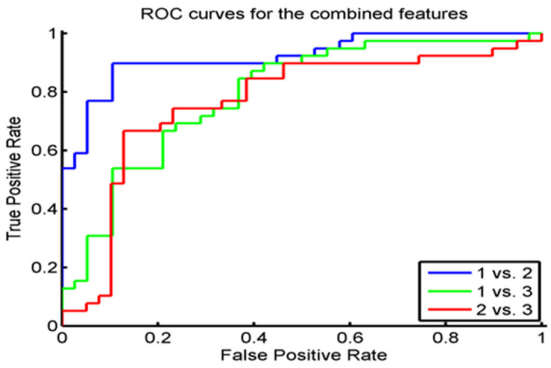

Figure 6: ROC curves of the combined features from the alpha-histograms and the Multifractal datasets using the best features

The major contributions of this study from the medical doctor's point of view is that the combined descriptor constructed after the cascaded approach, has significantly improved the overall classification accuracy of Emphysema images. The AUC value of 0.8559 also demonstrates the discriminating power of our approach in terms of separating the Emphysema with and without diseases; this is a great achievement since the separations between the normal and non-normal image samples are very important to the medical doctor or the radiologist.

4. CONCLUSION

This paper has presented a cascaded approach using the combined features of the multifractal and alpha-histograms descriptors for the classification of Emphysema in CT pulmonary images. The multifractal based descriptors demonstrate good performance in discriminating the normal Emphysema class from other pathological cases. Furthermore, the introduction of the alpha-histograms further improves the classification

results. The performances of the descriptors are measured by the overall classification accuracy and the area under the ROC curves. The results compared favourably well with the state-of-the-art measure for Emphysema, with an AUC of 0.8559 compared to 0.713. The proposed ideas significantly increase the classification accuracy, and confirm the effectiveness and robustness of the multifractal techniques in the classification of Emphysema images. The problem with the combined features is that the model complexity increases, which might slow the computational time and also increase the memory usage. The performance of the combined descriptors can be improved by parallelizing the classifier algorithms using the GPU parallel computing as this might improve the computational efficiency. Further effort would be to cascade the LBP-based approach with the multifractal techniques, and the results of the combined descriptors would be examined on the classification of Emphysema in CT images. The performances of the descriptors may be evaluated against other classification approaches.

5. ACKNOWLEDGMENT

The authors would like to thank Dr. Lauge Sorensen and other researchers for making available the online computed tomography Emphysema database used in this research.

6. CONFLICT OF INTEREST

There is no conflict of interest associated with this work.

REFERENCES

Chabat, D.H.F. and Yang, G. (2003). Obstructive lung diseases: texture classification for differentiation at CT. *Radiology*, 228(3), pp. 871–877.

Choi, E. and Lee, C. (2003). Feature extraction based on the Bhattacharyya distance. *Journal of Pattern Recognition Society*, 36, pp. 1703–1709.

Falconer, K. (2003). *Fractal Geometry-Mathematical Foundations and Applications*. 2nd ed. London: *Wiley*.

Gavrovska, A, Zajic and G, Reljin, I. (2013). Classification of prolapsed mitral valve versus healthy heart from phonocardiograms by multifractal analysis. *Computer and Mathematical Methods in Medicine*. 2013.

Hemsley, A, and Mukundan, R. (2009). Multifractal Measures for Tissue Image Classification and Retrieval. *11th IEEE International. Symposium and Multimedia*, pp. 618–623.

Ibrahim, M, and Mukundan, R. (2014). Multifractal Techniques for Emphysema Classification in Lung Tissue Images. *International Conference on Environment, Chemistry and Biology,* 78, pp. 115–119.

Ibrahim, M.A., Ojo, O.A. and Oluwafisoye, P.A. (2017). On Feature Selection Methods for Accurate Classification and Analysis of Emphysema CT Images. *International Journal of Medical Imaging*, *SciencePG,* 5(6), pp. 70-78.

Ibrahim, M.A., Ojo, O.A. and Oluwafisoye, P.A. (2017). Analysis of Emphysema Patterns Computed Tomography Image. *International Journal of Scientific & Engineering Research,* 8(12), pp. 2157-2168.

Mukundan, R. and Hemsley, A. (2010). Tissue Image Classification Using Multifractal Spectra. *International Journal of Multimedia, Data Engineering and Management*, 1(2), pp. 62–75.

Nilsson, E. (2007). Multifractal-based Image Analysis with applications in Medical Imaging. *Department of Computer Science, Umea University, Umea Sweden*, pp. 33–70.

Sorensen, L. and De-Bruijne, M. (2008). Texture Classification in Lung CT using Local Binary Patterns. *In: Proceeding of Medical Image Computing and Computer Assisted Intervention.*

Sørensen, L, De-Bruijne, M. (2009). Dissimilarity representations in lung parenchyma classification. *In: Proceeding of the Spie digital library Conference, Medical imaging*, Computer-Aided Diagnosis, 7260(27), pp. 1–12.

Sørensen, L., Shaker, S.B. and De-Bruijne, M. (2010). Quantitative Analysis of Pulmonary Emphysema using Local Binary Patterns. *IEEE Transaction in Medical Imaging*, 29(2), pp.559–569.

Sorensen, L., Nielsen, M. Lo, P., Ashraf, H., Pedersen, J. H. and De Bruijne, M. (2011). Texture-based analysis of COPD: a data-driven approach. *IEEE Transactions on Medical Imaging,*31(1), pp. 70–78.

Stojic, T., Reljin, I. and Reljin, B. (2006). Adaptation of multifractal analysis to segmentation of microcalcifications in digital mammograms. *Physics A. Statistics Mechanism and its Application*, 367, pp. 494–508.

Tay, C., Mukundan, R. and Racoceanu, D. (2011). Multifractal Analysis of Histopathological Tissue Images. *International conference on computer vision in New Zealand*, pp. 80–85.

Vasiljevic, J., Reljin, B. and Sopta, J. (2012). Application of multifractal analysis on microscopic images in the classification of metastatic bone disease. *Biomedical Microdevices*, 14, pp. 541–548.

Vehel, J.L. and Mignot, P. (1964). Multifractal Segmentation of Images. *Fractals, Image*, 2, pp. 371–378.

Wang, L. (2005). Support Vector Machines: Theory and Applications. *Berlin: Springer-Verlag*.

Zhang, H. (2009). A Novel Bayes Model: Hidden Naive Bayes. *IEEE Transaction. Knowledge in Data Engineering*, 21(10), pp. 1361–1371.

Zhang, H. and Su, J. (2008). Naïve Bayes for optimal ranking. *Journal of Experimental & theoretical Artificial Intelligence*, 20(2), pp. 79-93.